INSTITUTE OF PHYSICS PUBLISHING JOURNAL OF MICROMECHANICS AND MICROENGINEERING

J. Micromech. Microeng. **13** (2003) S45–S50 PII: S0960-1317(03)59954-5

X-ray detector based on a bulk micromachined photodiode combined with a scintillating crystal

J G Rocha[1], C G J Schabmueller[2], N F Ramos[1], S Lanceros-Mendez[3], M F Costa[3], A G R Evans[2], R F Wolffenbuttel[4] and J H Correia[1]

[1] Department of Industrial Electronics, University of Minho, Campus de Azurem, 4800-058 Guimaraes, Portugal
[2] Microelectronics Centre, Department of Electronics and Computer Science, University of Southampton, Southampton SO17 1BJ, UK
[3] Department of Physics, University of Minho, Campus de Gualtar, 4710-057 Braga, Portugal
[4] Laboratory of Electr. Instr., Delft University of Technology, Delft, the Netherlands

E-mail: gerardo@dei.uminho.pt

Received 24 February 2003, in final form 15 April 2003
Published 13 June 2003
Online at stacks.iop.org/JMM/13/S45

Abstract
In this paper we report on the design, fabrication, assembly and testing of an x-ray detector based on a bulk micromachined photodiode (BMMPD) with a cavity filled with a scintillating crystal. The x-ray photons that reach the detector are first converted to visible light by the scintillating crystal. The visible light is then detected by the BMMPD, producing an electric current with a value proportional to the incident x-ray intensity. Tests were performed using two x-ray setups: an experimental setup and a professional setup. The first was powered with a maximum voltage of 35 kV, and a current ranging to 1 mA, and the second was powered with voltages from 40 to 60 kV and currents ranging from 10 to 55 mA.

1. Introduction

Several medical imaging methods are digital, such as computed tomography, ultrasound and magnetic resonance, while conventional x-ray imaging remains an analog technique [1]. X-ray imaging techniques usually have very strict exposure requirements due to the narrow brightness depth of the traditional radiographic silver films. They also offer very few possibilities for image processing. On the other hand, digital radiography systems offer the possibility of imaging with a wider range of exposure requirements and provide an image that may be processed and displayed in a variety of ways.

The main advantages of digital radiographic systems may be divided into three classes:

- dose reduction;
- image processing and display in real time;
- flexibility in image storage and retrieval.

The first advantage of digital radiography is the possibility of dose reduction. In conventional radiology, the dose is determined by the sensitivity of the image receptor and the film brightness depth. In digital radiology, both these constraints can be relaxed. Dose reduction can be achieved by adjusting the dose to give the required signal-to-noise ratio in the image. Further reductions are possible by using the x-ray spectra that give the lowest dose for a given signal-to-noise ratio and by recovering any losses in contrast using digital techniques [2].

The second advantage of digital radiography is the possibility of changing the characteristics of the image during the medical evaluation; brightness and contrast can be adjusted after the x-ray session.

The third advantage of digital radiography is the possibility of image storage in a computer database and/or its fast transmission to long distances.

Having in mind the advantages of digital radiography relative to the traditional radiography, based on silver halide

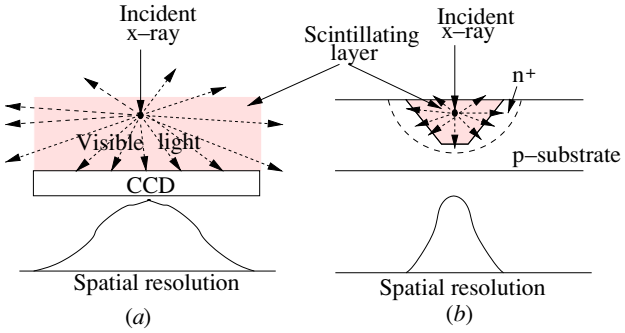

Figure 1. Spatial resolution of (*a*) a CCD with scintillating layer, and (*b*) a BMMPD with a scintillator.

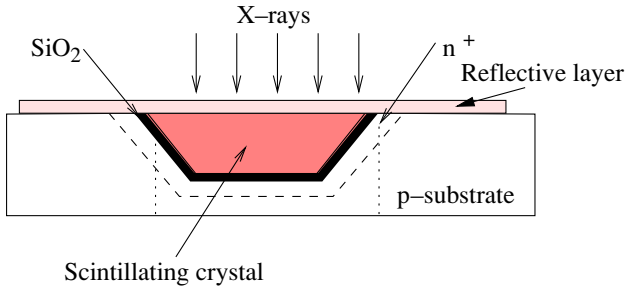

Figure 2. Diagram of the x-ray sensor based on a BMMPD.

Table 1. Properties of CsI:Tl as a scintillating material at room temperature [9].

Density (g cm^{-3})	4.51
Effective atomic number	54
Light yield (photon MeV^{-1})	65 900
Emission wavelength (nm)	560
Decay time (ns)	10^3

films [3], the main purpose of the present work is to validate a simple and efficient solution for an x-ray detector using electronic integration and micromachining technologies.

2. Background

One of the first x-ray sensors developed was based on a silicon charge coupled device (CCD) [4]. The silicon has a low x-ray absorption coefficient, but for each 1 keV of x-ray photons absorbed, about 277 electrons are excited [5]. This enables the construction of x-ray sensors with better sensibility than the traditional radiographic silver films. However, the small number of detected photons in the CCD results in a significant quantum noise [5]. In order to reduce the quantum noise, the radiation dose can be increased or the quantum efficiency of the sensor can be improved. The increase in the x-ray dose is obviously not desired for medical applications. The quantum efficiency of the sensor can be increased by adding a scintillating layer above the CCD. Since the x-rays are first absorbed by the scintillating layer, which has a high absorption coefficient, and then converted into visible (or near visible) light, the quantum efficiency of the detector is improved. A drawback of this approach is that the spatial resolution of the device is approximately equal to the thickness of the scintillator layer [6] (figure 1(*a*)). An increase of the scintillating layer thickness can be achieved, without decreasing the spatial resolution, by using bulk micromachined photodiodes (BMMPDs), as shown in figure 1(*b*). In this case, the light produced by the scintillator is confined to the corresponding BMMPD cavity. Previous attempts using similar methods have been described in [7]. These approaches are based on avalanche photodiodes implemented behind the wafer. The drawbacks of these methods—high bias voltages and loss of light through the lateral walls of the cavity—are overcome by our prototype.

3. Design

In medical imaging diagnosis, x-rays are produced with voltages from 25 to 120 kV, approximately. These voltages produce an intensity peak ranging from 10 to 100 keV. A standard silicon wafer (525 μm thick) only absorbs about 2.2% of the 100 keV x-ray energy. A 16.2 mm thick layer absorbs 50% of the same radiation, so that for practical applications each photodiode junction needs to be at least 20 mm thick, which is completely impractical [8]. Therefore, as pointed out in the previous section, an x-ray scintillation layer which converts x-rays into visible light is a good approach for increasing the quantum efficiency of the silicon detectors: a larger amount of x-rays are absorbed and converted into visible light, which can be detected by the silicon devices.

In the case of image acquisition by an array of BMMPDs filled with scintillating crystals, the light produced by each scintillator is isolated from its neighbors, reducing losses and cross-talk between adjacent detectors. Moreover, introducing a reflective layer for the visible wavelengths above the scintillator (in the x-ray path) confines the visible light inside the cavity of the BMMPD, increasing the efficiency.

Therefore, the device consists of a p-type silicon substrate, where a test cavity is made. The inner walls of the cavity are doped to form an n$^+$ region and the cavity is then filled with a scintillating crystal. Finally, a film of a reflective material is placed above the scintillating crystal, as shown in figure 2.

3.1. Scintillating crystal

This application requires a scintillating crystal with high light yield and reasonably fast decay time [9]. CsI:Tl satisfies both conditions. It has a peak emission wavelength of 560 nm which, combined with silicon devices, is one of the materials with the highest quantum efficiency [10]. Table 1 shows the most important properties of CsI:Tl as a scintillating material.

Figure 3 shows the x-ray absorption by a 400 μm thick layer of CsI:Tl in the range 10–100 keV, where 400 μm is the depth of the BMMPD cavity (see 4.1). The calculations are based on the mass energy-transfer and mass energy-absorption coefficients of the materials [11]. In this figure we can also observe the effect of the *k* edges of cesium and iodine at 35.9846 and 33.1694 keV, respectively.

3.2. Photodiode

For silicon, the penetration depth of light with $\lambda = 560$ nm is $\approx$0.75 μm [12]. To maximize the efficiency of the diode by minimizing recombination, the junction depth needs to be as shallow as possible. A junction depth of 0.1 μm has been calculated using SUPREM, a device simulator from Stanford.

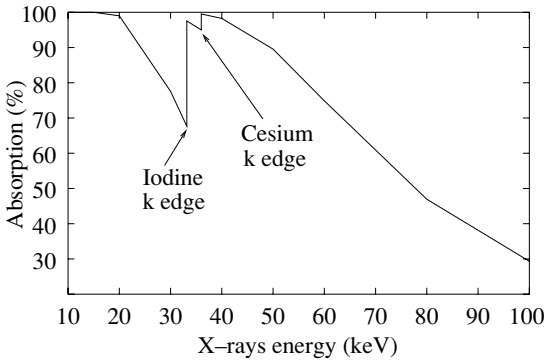

Figure 3. Absorption of a CsI:Tl crystal 400 μm thick.

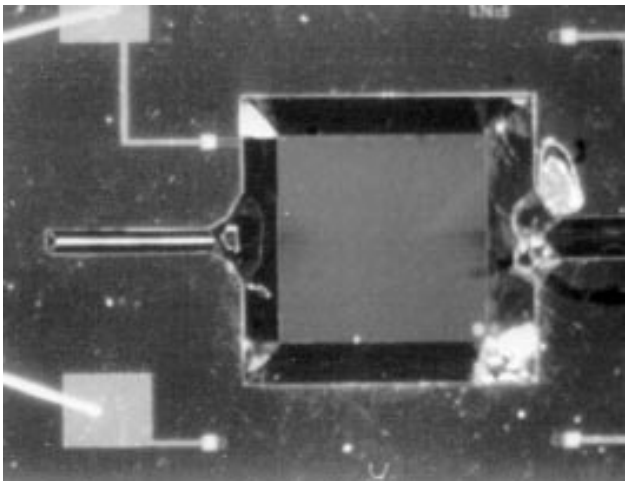

Figure 4. Diode detector with a cavity size of 2 × 2 mm^2.

4. Fabrication

4.1. Photodiode

For the fabrication of the BMMPD chip, a p-type silicon wafer is used. Two boron implantations onto the front (1×10^{14} cm^{-2}, 30 keV) and back (5×10^{15} cm^{-2}, 50 keV) respectively are implemented to assist the ohmic contact to the metal in later stages. The wafer is then covered with an oxide and nitride layer. Patterning the photoresist and dry etching the nitride and oxide layers leaves the mask for etching the cavity. The cavity is etched into the wafer with KOH. The nitride and oxide films are then stripped from the wafer. After the creation of the cavity using KOH, arsenic is implanted (1×10^{16} cm^{-2}, 50 keV) through a 40 nm thick oxide layer to form the pn diode. This oxide is then stripped off and a new 80 nm thick oxide layer is grown thermally to insulate the metal tracks for the diode connection and to act as an anti-reflection coating. The oxide is patterned with buffered hydrofluoric acid to create contact windows to the silicon. Layers of titanium and aluminum/silicon are then sputtered on the front and back of the wafer, respectively, and patterned on the front in order to fabricate the metal tracks. A picture of the chip is shown in figure 4. Three extra diodes were included in the design for test purposes.

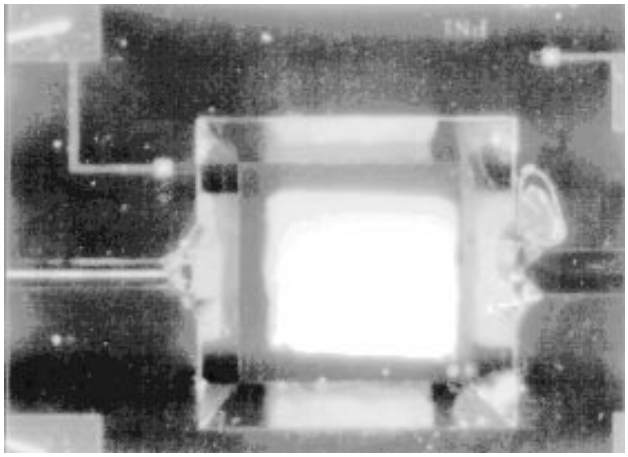

Figure 5. Diode detector filled with CsI:Tl.

Table 2. Physical properties of CsI.

Crystal class and space group	Cubic $Pm3m$ (221)
Unit cell lattice parameters, Å	4.566
Formulas per unit cell, Z	1
Molecular weight, amu	259.81
Density, g cm^{-3}	4.53
Melting point, K	898
Cold water solubility, g 100 g^{-1}	44.0
Elastic moduli, GPa	18
Shear moduli, GPa	7.3
Bulk moduli, GPa	12.6
Poisson's ratio	0.26
Flexure strength, MPa	5.6

4.2. Scintillating crystal

The scintillating crystal (CsI:Tl) is produced by Molecular Technology GmbH, Berlin, Germany. The main parameters of this single crystal are presented in table 2. When cut into thin sheets, cesium iodide may be bent into various shapes without fracturing, and it is reasonably soft and malleable [13]. Due to its elastic properties, a clamping pressure of 10 MPa is enough for transferring and fixing the crystal into the cavity without breaking. Nevertheless, this process induces some residual stresses within the material that reduces the optical transmissivity of the scintillator. So, after this step, it is necessary to anneal the scintillator in order to improve its optical transmissivity. The scintillating crystal must be a good absorber of x-ray photons, but it is also desirable that the produced visible light reaches easily the surface of the photodiode. The placement of the scintillating crystal inside the cavity, by means of a clamping pressure, does not degrade the x-ray absorption, but its transmissivity to visible light is reduced. Due to this factor, the annealing process becomes necessary. The annealing is performed at 340 °C during 2 h at a normal atmospheric pressure [14]. Figure 5 shows a picture of the chip after this step.

4.3. Reflective layer

As a final step, a film of reflective ink was deposited above the scintillating crystal. This film was deposited using a pressurized spray through a deposition mask.

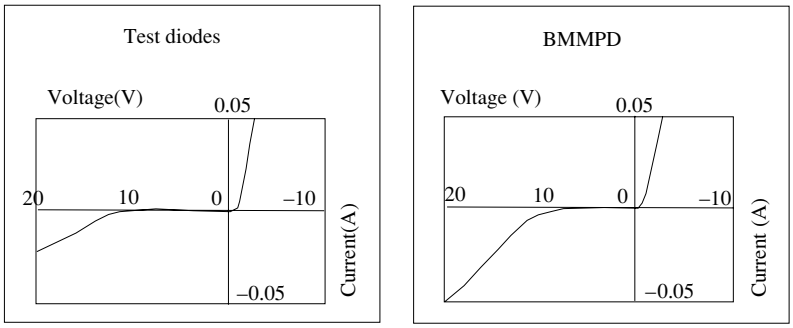

(*a*) (*b*)

Figure 6. Dark current *I–V* characteristics for a test diode 1 (*a*) and the BMMPD (*b*).

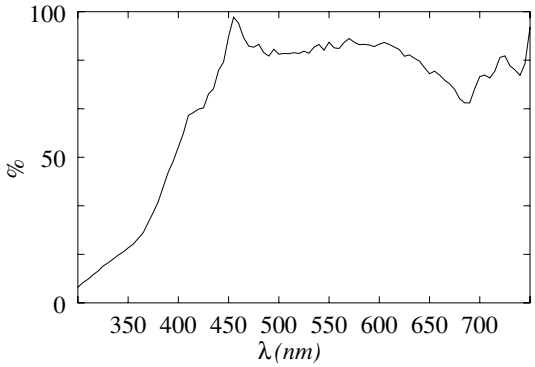

Figure 7. Spectral response of the BMMPD.

5. Test procedures and results

Current–voltage (*I–V*) characteristic curves for the diodes have been obtained using a Hewlett Packard 4155A four-probe analyzer. The characteristics of the three test diodes were measured in order to evaluate the BMMPD characteristics and performance. The *I–V* characteristic of the BMMPD (2 × 2 mm^2) was compared to one of the test diodes. As expected, the *I–V* characteristic of the BMMPD and the test diodes are similar, except for a softer breakdown knee in the BMMPD (figure 6). Furthermore, the fact that the BMMPD has a low reverse leakage current allows its use for light detection.

The spectral response of the BMMPD was measured using an Oriel spectral analyzer system motorized monochromator UV-VIS. The output current was measured using a Keithley 487 picoamperimeter/voltage source with no bias applied to the photodiode. Figure 7 shows the spectral response of the BMMPD from 300 to 750 nm normalized to the maximum current.

Table 3. Improvement in the transmissivity of CsI:Tl crystals after the annealing at 340 °C and atmospheric pressure.

Sample	Annealing time (h)	Transmissivity improvement (%)
A	1	5.8
B	2	12.9
C	3	1.9

Another experiment was carried out in order to improve the annealing step of the scintillator. In this experiment, three aluminum sheets were prepared with holes at their centers. The holes were filled with scintillator crystals using a clamping pressure of 10 MPa. The three aluminum sheets with the scintillators were then annealed respectively for 1, 2 and 3 h. The transmissivity of the CsI:Tl crystal before and after the annealing process was measured with the circuit of figure 8. The LED was driven with a 5 kHz wave. This 5 kHz light modulation allows the filtering of the noise caused by the environment lights. The results obtained with this circuit are given in table 3. After 2 h of annealing, the improvement in the scintillator transmissivity is approximately 13%. Figure 9 shows sample B after the annealing step. The low transmissivity values of sample C are probably due to oxidation and cracks of the crystal.

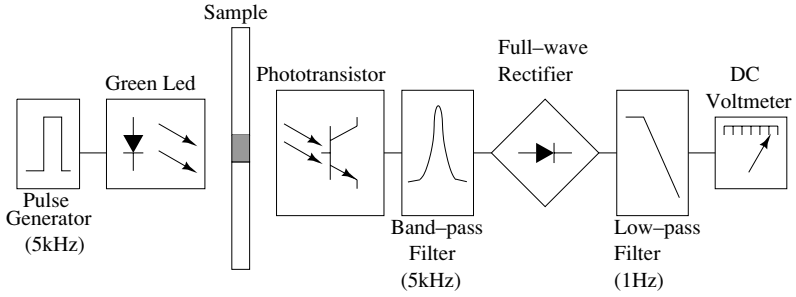

Figure 8. Circuit used for transmissivity measurements.

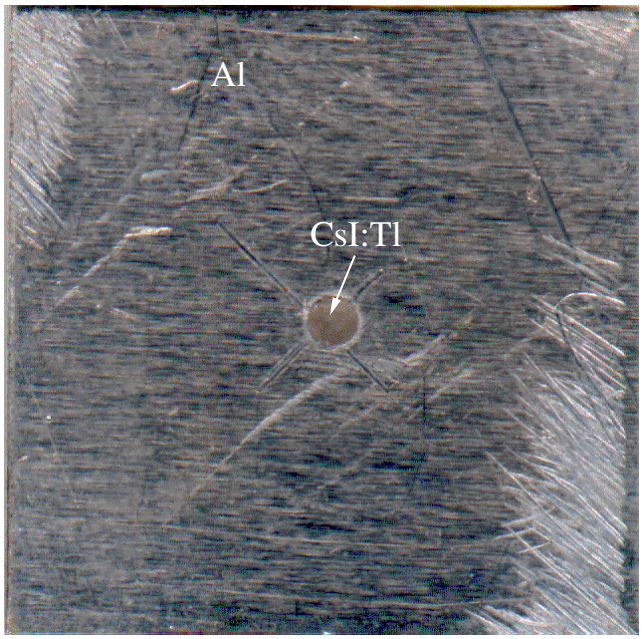

Figure 9. Aluminum sheet with CsI:Tl after 2 hours annealing time.

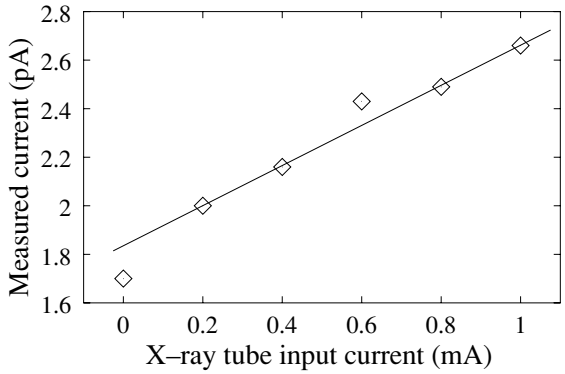

Figure 10. Experimental results (squares) of the detector with an x-ray tube input voltage of 35 kV. The line is used to guide the eyes.

The first x-ray test was performed using an x-ray tube (Leybold) with molybdenum anode, with characteristic radiation $K_\alpha = 17.4$ keV and $K_\beta = 19.6$ keV. The tube was powered with a voltage of 35 kV, and a current ranging to 1 mA. Figure 10 shows the measured values.

The second x-ray test was made with an x-ray tube from Phillips with a copper ampoule and a molybdenum anode. The tube was powered from 40 to 60 kV in voltage and 10–55 mA in current. For thermal limitations inside the tube, the maximum allowable current was 40 mA at 50 kV and 20 mA at 60 kV. Figure 11 shows the results.

In both cases (figures 10 and 11) a linear relationship (within experimental errors) between the input current of the x-ray tube and the response of the BMMPD device is obtained. As a curiosity, the x-ray tubes for dental radiography, using traditional films, are powered with a voltage near 70 kV and a current near 10 mA [3], i.e. a power about 20 times higher than that used in our first experiment.

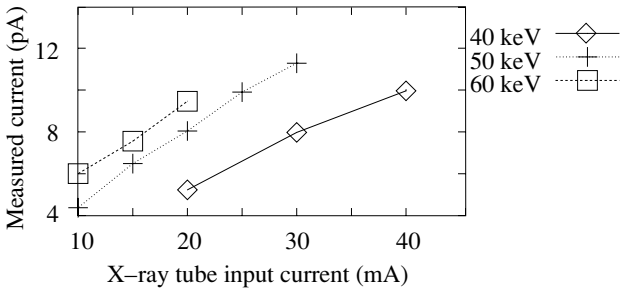

Figure 11. Experimental results of the detector with an x-ray tube input voltage ranging from 40 to 60 keV. The lines are used to guide the eyes.

6. Conclusion

We have designed, fabricated and tested a device based on a BMMPD and a scintillating crystal. This approach is found to be suitable for making x-ray detectors as a linear relationship has been found between the x-ray signal intensity and the output response of the device. An advantage of this architecture is that the photodiode cavity allows us to increase the scintillator thickness without decreasing the spatial resolution of several detectors, when placed together. So, for x-ray imaging, it can improve the performance of a CCD with a scintillating layer on top.

For future work, an array of 8×8 photodiodes will be placed on a new chip.

Acknowledgments

This work was supported by the Foundation of Science and Technology, Portugal: FCT-CTM/POCTI/33751/1999 and Grant-BD SFRH/BD/1296/2000.

References

[1] Kleymann P *et al* 2000 An x-ray imaging pixel detector based on a scintillating guides screen *IEEE Trans. Nucl. Sci.* **47** 1483–6
[2] Smathers R L and Brody W R 1985 Digital radiology: current and future trends *Br. J. Radiol.* **58** 285–307
[3] Selman J 1994 *The Fundamentals of X-rays and Radium Physics* 8th edn (Illinois USA: Charles C Thomas)
[4] Nelvig P *et al* 1992 Sens-a-ray: a new system for direct intraoral radiography *Oral Surg. Oral Med. Oral Path.* **74** 6
[5] Fröjdh C *et al* 1998 Simulation of the x-ray response of scintillator coated silicon CCDs *IEEE Trans. Nucl. Sci.* **45** 374–8
[6] Rowlands J A 1998 Current advances and future trends in x-ray digital detectors *IEEE Instrum. Meas. Mag.* **1** 26–8
[7] Allier C P *et al* 2001 Thin photodiodes for a neutron scintillator silicon-well detector *IEEE Trans. Nucl. Sci.* **48** 1154–7 and references therein
[8] Rocha J G and Correia J H 2001 A high-performance scintillator-silicon-well x-ray microdetector based on DRIE techniques *Sensors Actuators* A **92** 203–7
[9] Valentine J *et al* 1991 Temperature dependence of absolute CsI(Tl) scintillation yield *IEEE Nucl. Sci. Symp. Conf. Rec.* 176–82

[10] Smith S T *et al* 1999 Evaluation of a CMOS image detector for low cost and power medical x-ray imaging applications *Proc. SPIE* vol 3659 pp 952–61
[11] Seltzer S M 1993 Calculations of photon mass energy-transfer and mass energy-absorption coefficients *Radiat. Res.* **136** 147–70
[12] Wilson J *et al* 1989 *Optoelectronics, an Introduction* (Englewood Cliffs, NJ: Prentice-Hall)
[13] Crannell C J, Kurz R J and Viehmann W 1974 Characteristics of cesium iodide for use as a particle discriminator for high-energy cosmic rays *Nucl. Instrum. Methods* **115** 253–61
[14] Vieux G and Rougeot H 1989 Input screen scintillator for a radiological image intensifier tube and a method of manufacturing such a scintillator United States Patent 4803366